Available online at www.sciencedirect.com
ScienceDirect
Journal of Bionic Engineering 10 (2013) 292–304

Turning in a Bipedal Robot

Jau-Ching Lu, Jing-Yi Chen, Pei-Chun Lin

Department of Mechanical Engineering, *National Taiwan University*, *Taipei* 106, *Taiwan*

Abstract

We report the development of turning behavior on a child-size bipedal robot that addresses two common scenarios: turning in place and simultaneous walking and turning. About turning in place, three strategies are investigated and compared, including body-first, leg-first, and body/leg-simultaneous. These three strategies are used for three actions, respectively: when walking follows turning immediately, when space behind the robot is very tight, and when a large turning angle is desired. Concerning simultaneous walking and turning, the linear inverted pendulum is used as the motion model in the single-leg support phase, and the polynomial-based trajectory is used as the motion model in the double-leg support phase and for smooth motion connectivity to motions in a priori and a posteriori single-leg support phases. Compared to the trajectory generation of ordinary walking, that of simultaneous walking and turning introduces only two extra parameters: one for determining new heading direction and the other for smoothing the Center of Mass (COM) trajectory. The trajectory design methodology is validated in both simulation and experimental environments, and successful robot behavior confirms the effectiveness of the strategy.

Keywords: turning, biped, humanoid, trajectory planning, robot

doi: 10.1016/S1672-6529(13)60225-5

1 Introduction

Recently, humanoid robotics has drawn great attention in the robotics community because it raises an important and challenging issue in bipedal locomotion[1]. Unlike wheeled robots, which are designed for moving on flat ground, legged platforms are used on uneven terrain. Because of similar morphology, bipedal robots are particularly suitable for the deployment in the artificial environments that are designed by and for human beings. Among the tasks to create a movable bipedal robot, gait generation is a fundamental yet crucial task on the control side. Generally, bipedal walking gaits can be categorized into two motions: straight walking and turning, and the latter can further be categorized into turning in place and simultaneous walking and turning. While most research work focuses on straight walking[2–8], some results on turning have also been reported. For example, Lim *et al*. proposed a method that uses 7th-order polynomials to generate waist and foot trajectories for turning with an arbitrary Zero-Moment-Point (ZMP) setting[9]. However, very limited information was provided on the complete smooth trajectory generation. Kajita *et al*. proposed a 3-D Linear Inverted Pendulum Model (LIPM) for bipedal walking pattern generation, but no information was revealed about the complete gait generation or about the experimental validation[10]. Various research groups have designed turning in place from kinematic models with robots programmed either to turn their feet first[11,12], or to turn their waists first[13], or mixed behavior[14]. However, the motivation and reason for choosing the specific method are discussed very limitedly, and no comparison of these strategies has been made. Besides the standard turning motion, Shi *et al*. proposed a method for online omni-directional walking pattern generation, but no information was revealed about the complete gait generation or about the experimental validation[15]. In contrast, some groups used human motion as their reference to generate a human-like walking and turning gait[16,17], or even dancing[18,19] and Chinese Kung-Fu and Tai-ji practicing[20]. This approach yields very fast motion generation when the dynamic properties of the human and the robot can be easily mapped. ASIMO, developed by Honda Co. Ltd. demonstrated high-speed simultaneous walking and

Corresponding author: Pei-Chun Lin
E-mail: peichunlin@ntu.edu.tw

turning by tilting its body, but unfortunately no detailed information was revealed[21,22]. Recently, by knowing the friction properties of the ground, robots of the HRP series, developed by the National Institute of Advanced Industrial Science and Technology (AIST) in Japan[23,24], and WABIAN, developed by Waseda University[25], could perform a novel fast-turning technique called flip-turn, or twirl.

In this paper, we report on the trajectory generation, kinematic simulation, and experimental evaluation of general turning behavior in a bipedal robot. We propose and experimentally validate a new method of standstill turning that uses two-step body turning, which can yield a larger turning angle in one complete turning stride. By implementing this method and two other methods reported by other researchers (*i.e.*, body-first and leg-first), we conducted an experiment-based comparison. Furthermore, we report on the complete trajectory generation and experimental validation of simultaneous walking and turning based on the 3D LIPM and ZMP criteria, including the considerations of the robot moving in both the single-leg support phase and the double-leg support phase (hereafter are referred to as the "SS phase" and the "DS phase," respectively). To the best of our knowledge, this behavior has not been clearly and thoroughly reported.

Section **2** reports on the methodology of trajectory generation for both turning in place and simultaneous walking and turning. The detailed steps of all behaviors are addressed and compared. Section **3** shows the simulation and experimental results of developed turning behaviors, and the simulation used for checking stability and feasible operating range before the experiment is conducted. Section **4** reports the conclusions of our work.

2 Methods

Development of turning behavior is strongly related to the mechanism structure of the physical robot. Fig. 1a shows the robot used for empirical implementation and experimental validation of turning behavior. Fig. 1b shows the mechanism structure of the robot, which has 12 active Degrees of Freedom (DOFs) on the legs: 3 in each hip, 1 in each knee, and 2 in each ankle. This particular arrangement of DOFs is adopted in many humanoid robots, and it is very similar to the human structure as well. Table 1 lists the operating ranges of all leg joints on the robot.

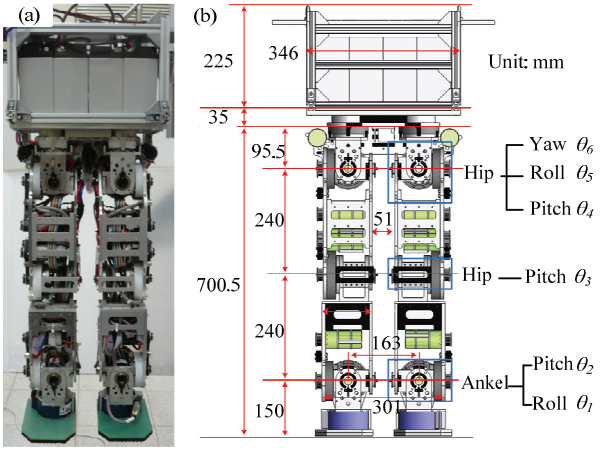

Fig. 1 The bipedal robot for experimental evaluation. (a) Photo; (b) DOFs and dimensions of the robot.

Table 1 Allowable operating range of leg joints

Leg joints		Theta range (°)
Hip	Pitch: θ_6	−90 – 37.5
	Roll: θ_5	−29.8 – 23.9
	Yaw: θ_4	−43.2 – 43.2
Knee	Pitch: θ_3	−8.6 – 131.9
Ankle	Pitch: θ_2	−108.6 – 51.5
	Roll: θ_1	−29.8 – 22.4

Generally, turning behavior can be classified into two categories: turning in place and simultaneous walking and turning. The former refers to the scenario when the Center of Mass (COM) of the robot remains roughly in the same position after turning. Owing to the static characteristic of COM motion, this behavior is usually initiated when the robot is in a standing posture. In contrast, if the robot originally has a forward motion, such as in walking, the initiation of turning introduces lateral motion to the robot's body, resulting in simultaneous walking and turning motion.

Stability is one of the crucial issues to consider, and the ZMP criterion is adopted here as the basis for judgment. To balance the force and momentum for stable locomotion, the ZMP of the robot is set to be located within a supporting region, which is either the area formed by one foot in the SS phase or the area enclosed by two feet in the DS phase. Note that in the case of turning in place, the ZMP is roughly equal to the center of pressure[26], since the motion is most likely quasi-static. Also note that although in some dynamic locomotion (such as motion with an aerial phase), the ZMP is not necessarily required to be located within the support plane at all time, here this requirement is met for

simplicity.

Measurement of the ZMP requires multi-axis force transducers installed around the ankle. In order to plan the turning trajectory in simulation without empirically involving the physical platform, a LIPM is used to represent the robot, as shown in Fig. 2, in which the robot body is modeled as a point mass and the leg is modeled as a massless link. To further simplify the motion dynamics, the ground-contact leg is assumed to have no slippage, and the height of COM is set at a constant, Z_c, to eliminate the nonlinear terms in the pendulum model, as previous approaches have done[26]. In this case, the governing equation of spatial COM motion can be decoupled and the equation of forward motion can be represented as

$$\ddot{x}(t) = \frac{Z_c}{g} x(t), \tag{1}$$

where g is the gravity constant. Note that the equation of lateral motion is in the same form, with a change of variable from $x(t)$ to $y(t)$.

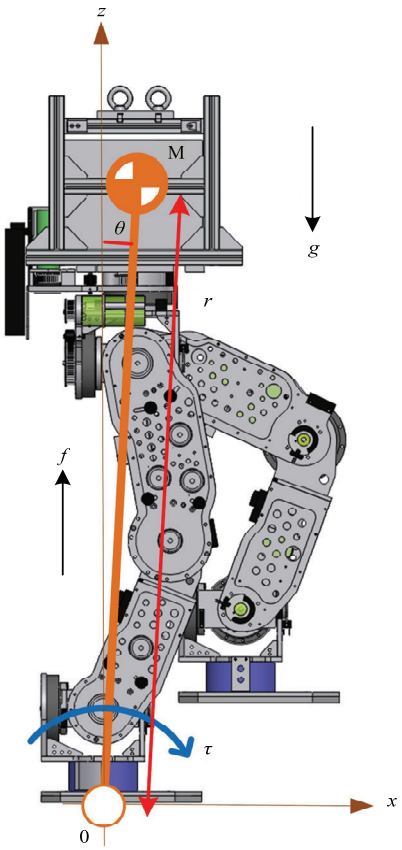

Fig. 2 The robot is modeled as an inverted pendulum in the motion design process.

2.1 Turning in place

The motion of turning in place consists of several procedures, as shown in Fig. 3. Assume the motion begins from ordinary standing posture, as shown in Fig. 3a, in which both legs are straight down and the distance between the ankles is equal to the distance between the hips, which is denoted as $Y_{\Delta ZMP}$. First, slightly bend the knees of the robot, as shown in Fig. 3b, so the leg joints are away from singularity. Second, move the upper body in the lateral direction to shift the ZMP onto the leg that will act as the supporting leg during turning, as shown in Fig. 3c. Thus, the ZMP is shifted accordingly, with the distance half of $Y_{\Delta ZMP}$. Next, the robot turns with turning angle θ in one of three methods that are body-first (Fig. 3(d-f-I)), leg-first (Fig. 3(d-f-II)) and body/leg-simultaneous (Fig. 3(d-f-III)). Finally, after turning, the robot shifts its COM back to the area between the two feet (Fig. 3g), and then stands up in an ordinary standing posture (Fig. 3h).

In the body-first method, first, the robot rotates its upper body to the desired orientation with angle θ (Fig. 3(d-I)). Next, the ZMP of the robot shifts to the rotated leg (Fig. 3(e-I)), which then acts as the supporting leg. Finally, the original supporting leg rotates to align itself to the direction of the rotated body (Fig. 3(f-I)).

In the leg-first method, first, the non-supporting leg moves to a position with angle θ and the distance from $Y_{\Delta ZMP}$ to ZMP, as shown in Fig. 3(d-II). Next, the ZMP shifts to the moved leg without changing the orientation of the robot body till the hip of the moved leg is at a distance half of $Y_{\Delta ZMP}$ from the right knee and with the same angle θ as the turning angle, as shown in Fig. 3(e-II). With the ZMP on the moved leg, the robot then rotates its body and left leg to the final orientation, as shown in Fig. 3(f-II). Owing to the same geometrical constraint as that in leg-first method, the leg rotates slightly backward to achieve the turning motion.

In the body/leg-simultaneous method, first, by rotating both yaw DOFs on the hips $\theta/2$, the robot rotates its body with angle $\theta/2$ and simultaneously positions its moving leg to the final location with angle θ, as shown in Fig. 3(d-III). Next, the ZMP shifts to the turned leg without altering body orientation, as shown in Fig. 3(e-III). Finally, by rotating both yaw DOFs on the hips $\theta/2$ again, the robot rotates its body with angle $\theta/2$ accordingly, and both feet align with each other, as shown in Fig. 3(f-III).

The three turning methods described above are suitable for different conditions. The factors to be considered include the motion before/after turning, the spatial constraints imposed by surroundings, and the motion constraints imposed by mechanisms of the robot. If walking follows the turning immediately, the body-first method is the best choice. In this method, the body is set to turn and face the final direction in the very first phase of the turning motion. Thus, after the ZMP shifts to the supporting leg, instead of bringing the feet back together, as shown in Fig. 3(f-II), the moving leg can be set to move forward as in the ordinary stride of walking. In contrast, if either the leg-first method or the body/leg-simultaneous method is used in this case, another transition stride should be deployed to bridge the motion.

If the space behind the robot is very tight or the overall motion is a combination of walking, stopping, and turning, the leg-first method is preferred, since the leg always moves forward, avoiding the backward-moving step used in the body-first or body/leg-simultaneous methods, as shown in Fig. 3(d -I) or Fig. 3(d-III). In the former case, the tight space may result in collision. In the latter case, the overall motion is not efficient because it involves a combination of forward and backward motion. Note that the behavior of a backward motion step in the body- first or body/leg-simultaneous method results from the setting of the supporting leg in these two methods: if the robot performs right turning, the left leg is used as the supporting leg; if the right leg is set as the supporting leg, the body and the left leg should rotate and move forward, which matches the desired motion pattern. However, this method results in the collision of the knees because the knee is bent forward during the turning motion (in walking, as well, to avoid leg motion singularity). As a result, for turning right, the left leg is set as the supporting leg, and the motion sequence shown in Fig. 3(d-f-I) or Fig. 3(d-f-III) is used, during which the knees move away from each other. In both methods, the rotation center is set at the point with half of the distance from $Y_{\Delta ZMP}$ to the ZMP, so the moving leg can rotate freely with an arbitrary turning angle, as shown in Fig. 3(d-I) or Fig. 3(d-III), without the necessity of enlarging the distance between the feet.

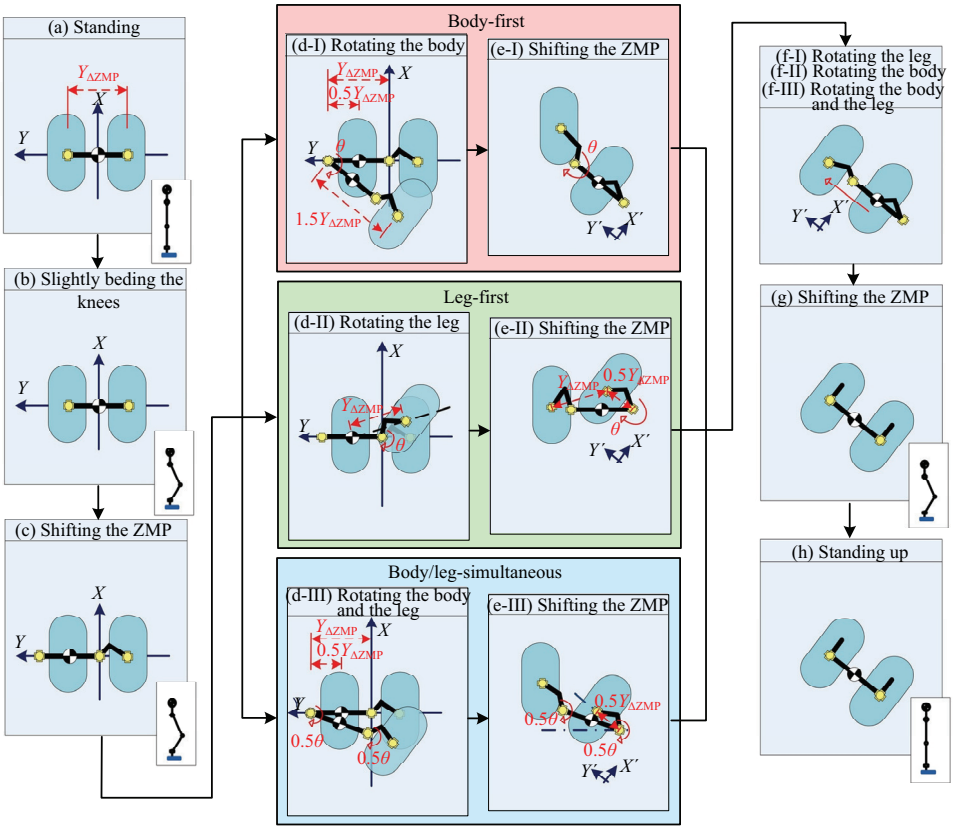

Fig. 3 Procedures for the robot to perform turning in place, which include those of all three methods reported in this paper.

The body/leg-simultaneous method is the best candidate when a large turning angle is desired. For given turning angle θ of the robot, one of the hip yaw DOFs (depending on right-turn or left-turn) has to rotate the same amount in the body-first method and the leg-first method. In contrast, both hip yaw DOFs rotate half of θ in the body/leg-simultaneous method, as shown in Fig. 3(d-III) and 3(e-III). Because the hip yaw DOF has a fixed range of motion, compared to the former two methods, the latter method can perform turning with doubled range of turning angle in one turning action. For experimental validation, the robot has a range of yaw angle from −43° to 43°, so it can turn −86° to 86° in one turning stride at maximum if the body/leg-simultaneous method is used.

In some scenarios, the choice of which turning method is suitable may not be obvious, and it may require further analysis. For example, the robot may be programmed to perform some tasks in front of a table or a bench, and after finishing the tasks, the robot should turn at least 90° and walk away. This scenario happens quite often. The body-first method has better motion continuity and the body/leg-simultaneous method has fewer turning strides. Thus, the judgment can be made based on the required time of motion or energy.

2.2 Simultaneous walking and turning

Development of the simultaneous walking and turning method is based on the ordinary straight walking pattern, thus, the design of the walking gait is introduced briefly first. Bipedal walking involves two phases, the SS phase and the DS phase, which alternate. In the SS phase, the COM moves according to the LIPM. Thus, both forward motion $x(t)$ and lateral motion $y(t)$ of the robot's COM are governed by the solution of Eq. (1), where $x(t)$ is listed as the exemplary presentation

$$x(t) = x(0)\cosh\left(\sqrt{\frac{g}{Z_c}}t\right) + T_c\dot{x}(0)\sinh\left(\sqrt{\frac{g}{Z_c}}t\right). \quad (2)$$

With given initial position and forward/lateral velocity, the motion in the SS phase can be predicted thoroughly according to Eq. (2). During motion, the ZMP of the LIPM is fixed at the contact point, so ZMP is located within the supporting region for stable motion. In the DS phase, the COM is supported by two massless links, as shown in Fig. 4a. To maintain the motion continuity from and to the SS phases, the 5th-order polynomial,

$$\sum_{i=0}^{5} a_i x(t)^i = 0 \quad (3)$$

is used to generate the COM trajectory in the DS phase. With the given initial and final displacements, velocities, and accelerations provided by the two SS phases before and after this specific DS phase, the six coefficients, a_i (i = 0, 1, …, 5) can be solved. During the motion, the ZMP shifts from the contact point of the original supporting leg to the new one. Note that in the stable and periodic COM motions, the initial and final states bridging the DS and SS phases are identical in the forward direction and the same in magnitude but opposite in direction in lateral motion. As a result, the continuous and periodic COM trajectory can be quantitatively defined, as illustrated in Fig. 4b. Also note that the time and spatial composition of the SS phase and the DS phase can be varied to generate different gaits. Because the forward motion is mainly generated in the SS phase, with a given period (time of SS + DS), the shorter DS phase yields faster forward speed. However, because the COM shift between two supporting legs is executed in the DS phase, the faster shifting also indicates more dramatic motion, which may result in instability. Besides the COM trajectory, foot trajectory should be planned as well. The foot is moved along with the moving leg to the next ground contact point during the SS phase. By

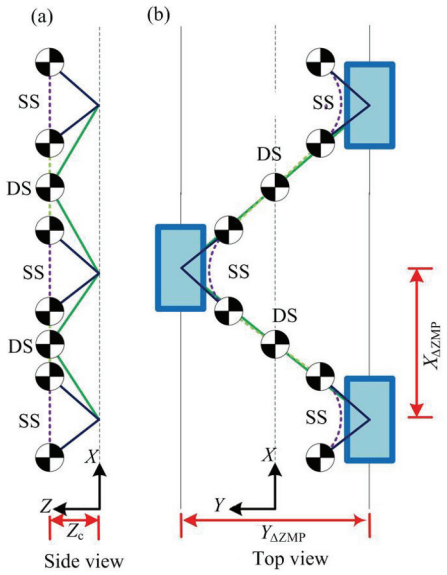

Fig. 4 Straight walking of the robot, during which it is modeled as an inverted pendulum.

setting a desired highest lifting height (with zero velocity and acceleration) at the middle point of foot trajectory, the foot trajectory can be created and combined by two 5th-order polynomials with preset initial, middle, and final foot positions, velocities, and accelerations. With the computed COM trajectory and trajectories of both feet versus time, the relationship between the joint angles of the legs and time can be computed by standard inverse kinematic procedures[14,27].

The motion pattern of simultaneous walking and turning is basically similar to that of the straight walking described in the previous paragraph. The major difference lies in the involvement of the body orientation change in the former case. This orientation change can be set either in the SS or the DS phase, or in both. In the current work, this change is set to execute in the DS phase but not in the SS phase for several reasons. Intuitively, the robot in the SS phase should move according to the inverted pendulum owing to the similarity of the walking and turning motion to the straight walking motion. Because the COM of the empirical robot does not directly locate on top of the supporting leg like the inverted pendulum, if the body turns in the SS phase, the mapping between the empirical robot and the inverted pendulum changes. This action also requires ground friction force to support the torque generated by the turning motion. In addition, the stable region in the DS phase is significantly larger than that in the SS phase. As a result, the body orientation change is set to execute in the DS phase.

The motion of simultaneous walking and turning is composed of several steps, as shown in Fig. 5a. Without the loss of generality, θ right turning is used as the example for the following description. The initial condition of this motion is straight walking, as shown in Fig. 5b. After the robot just finishes its *i*th SS phase supported by the right leg, SS_i, and begins its DS phase, DS_i, the body orientation starts to change direction while the COM shifts from the right leg to the left leg. The body orientation change is finished just before the end of the DS_i phase. In the next SS_{i+1} phase supported by the left leg, the trajectory of the inverted pendulum is rotated and scaled for two purposes: to align the body motion to the new forward direction, as shown in Fig. 5b; and to provide enough spatial space for generating a smooth trajectory in the DS phase. The orientation of the right foot is changed simultaneously, aligning it to the new forward direction. After the right leg contacts the ground, the motion of the following DS_{i+1} phase is just like that in ordinary walking, and the only difference is that both feet are not aligned in the same direction. Next, in the ordinary SS_{i+2} phase, the motion is set to move in the pendulum motion, the same as that in ordinary straight walking, but the left foot simultaneously changes its direction toward a new forward direction. After this step, the motion is totally the same as straight walking if no further turning is required.

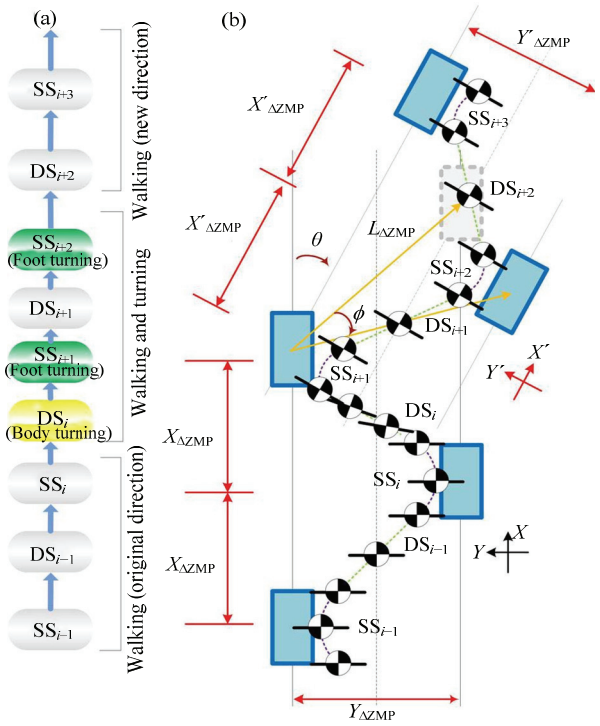

Fig. 5 Motion sequence of simultaneous walking and turning of the robot, during which it is modeled as an inverted pendulum.

There exists several computation details different from those in straight walking. As mentioned in the previous paragraph, the pendulum trajectory in the SS_{i+1} phase is deformed for turning, as shown in Fig. 5b. To ease the process of trajectory design, the forward and lateral components of the pendulum motion in the SS_{i+1} phase are linearly scaled down by the same tuning parameter, *K*, to the original motion computed in straight walking. Assuming that the forward and lateral walking trajectories in the SS_i phase are denoted as x_{SS_i} and y_{SS_i}, the distances in the SS_{i+1} phase are represented as

$$\begin{aligned} x_{SS_{i+1}} &= Kx_{SS_i}, \\ y_{SS_{i+1}} &= Ky_{SS_i}. \end{aligned} \tag{4}$$

In addition, the pendulum motion is set to align with a new forward direction; thus, the trajectory computation is executed in the rotated $x'y'$ coordinate frame, which is θ clockwise to the original xy coordinate frame, as shown in Fig. 5b. Next, similar to the computation strategy used in straight walking, the trajectory in the DS_i phase in between is generated by the 5th-order polynomial with boundary conditions provided by the SS_i phase and the SS_{i+1} phase. Because the motion in the SS_{i+1} phase determines the polynomial in the DS_i phase, the effect of K should be discussed. Fig. 6 plots the trajectories with four different settings of K. The blue curve and green curve represent COM trajectories in the SS_i phase and SS_{i+1} phase, respectively. Because it only affects the SS_{i+1} phase, the blue curves remain the same in all four plots. The figure clearly shows that the trajectories change in the DS_i phase according to the change of K. When K is small, the trajectory can be connected with less direction change. Thus, 0.25 is selected as the parameter value. While the right foot rotates θ in the SS_{i+1} phase in order to align to the new forward direction, the right foot can actually be positioned arbitrarily. To simplify the computation process, the distance between the feet, $L_{\Delta ZMP}$, a vector sum of $X_{\Delta ZMP}$ and $Y_{\Delta ZMP}$, is set the same as that in the other strides. Given the same traveling distance, the dynamics of the robot in this specific DS_i phase will be similar to that in other DS phases. As a result, the only parameter that needs to be introduced is the angle of the right foot with respect to the left foot, ϕ, as shown in Fig. 5b.

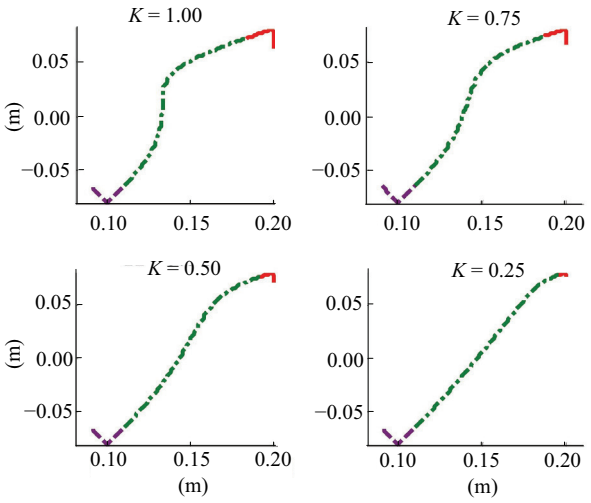

Fig. 6 Variations of the COM trajectory with scaling factor K.

3 Results

The method of generating COM trajectories in both single-leg and double-leg support phases is reported in section **2**. Foot trajectories are given, and joint trajectories of the legs can be derived by standard inverse kinematics. The proposed algorithm was evaluated first in simulation to make sure that (i) the motion was stable by checking whether the ZMP trajectory was completely within the supporting region and (ii) the joint trajectory was feasible to execute in the empirical robot. Then, the algorithm was evaluated experimentally in the empirical robot. Table 2 lists the parameters used in these evaluations.

Table 2 Motion and trajectory parameters used in simulation and experiments

Parameters	Z_c (m)	$X_{\Delta ZMP}$(m)	$Y_{\Delta ZMP}$ (m)	θ(°)	ϕ(°)
Value	0.5779	0.1	0.163	30	10
Parameters	K	DS phase (s)	SS phase (s)	SS $X_{COGDist}$ (m)	SS $Y_{COGDist}$ (m)
Value	0.25	1.8	3.6	0.02	0.0326

3.1 Simulation

Simulation is executed in Matlab and mainly used to check whether the ZMP trajectory is located within the supporting region. Fig. 7 shows the simulation results of turning in place, in which (I), (II) and (III) represent the body-first, leg-first, and body/leg-simultaneous, respectively. The upper figures are illustrative plots captured at exemplary moments of robot motion during turning. Leg configurations and COM and ZMP trajectories are plotted. Complete simulation of the above three methods can be found in the Media Extensions associated with this paper. To ensure that the ZMP is located within the supporting region the whole time, the right figures plot the ZMP and supporting region for each step of the turning motion. The green curves represent the overall ZMP trajectories in the turning motion, and the black hollow circle and orange area represent the COM and supporting region at each specific motion step, respectively. The figure clearly shows that the ZMP at each step is stably located within the supporting region, which grants the motion stability in regard to the pendulum model.

Fig. 8 shows the simulation result of simultaneous walking and turning. In the simulation, the robot first walks straight for 3 steps followed by a 30° right turn, and then walks straight for another step. The left figure in

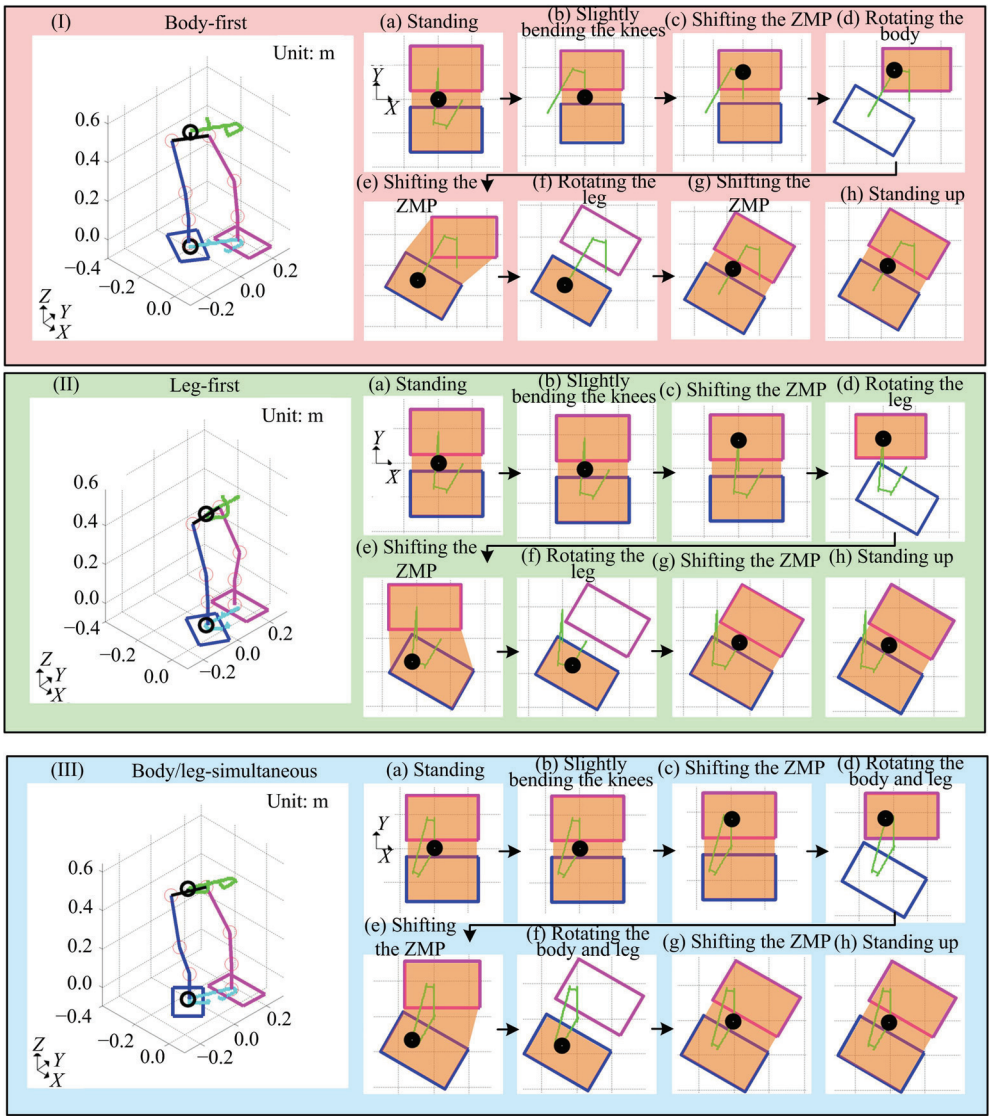

Fig. 7 Simulation of the robot performing turning in place, where (I), (II), and (III) are body-first, leg-first, and body/leg-simultaneous methods, respectively, the same notations as discussed in section **2.1** and also shown in Fig. 3. The left sub-figures are illustrative plots captured at exemplary moments of robot motion during turning. The right sub-figures plot the ZMP trajectories and the supporting regions during all steps in the turning motion.

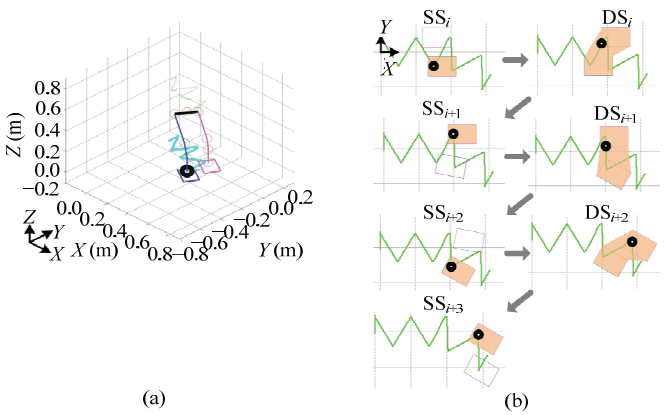

Fig. 8 Simulation of the robot performing simultaneous walking and turning. (a) An illustrative plot captured at exemplary moments of robot motion during turning; (b) the ZMP trajectories and the supporting regions during all steps in the turning motion.

Fig. 8 is an illustrative plot captured at an exemplary moment of robot motion during turning. The leg configurations and trajectories of the COM and ZMP are plotted. The complete simulation can also be found in the Media Extensions associated with this paper. The right figure plots the ZMP and the supporting region. The green curves, hollow black circle, and orange region are the same as before. Because the ZMP trajectory is located within the supporting region, the planned COM trajectory is stable and can be used for experimental evaluation.

Like human joints, all the joints of robot legs have bounded operating ranges, and one of the purposes of simulation is to check whether the designed joint trajectories exceed feasible limits. Table 1 lists the operating ranges of all leg joints. Fig. 9 plots the designed trajectories of all joints for the simultaneous walking and turning motion, confirming that the designed trajectories are feasible in terms of joint limit constraints. Note that the feasible turning range of each stride is determined by the method used (body-first, leg-first, or body/leg-simultaneous) and the operating range of the yaw joint. The current robot has about a 40° feasible operating range in both directions, and that implies that at least three strides are required for a 90° turn if using the body-first or leg-first method. In contrast, two strides are enough if using the body/leg-simultaneous method.

3.2 Experiment

The bipedal robot shown in Fig. 1a was used for experimental evaluation. The weight of the robot is 60 kg. A real-time embedded control system (sbRIO-9642, National Instruments) running at 500 Hz controlled motion. The designed trajectories are directly loaded from Matlab into LabVIEW for motion generation.

Fig. 10 shows experimental snapshots of the robot turning in place, where (I), (II), and (III) are the shots of the body-first, leg-first, and body/leg-simultaneous methods, respectively. Complete videos of the above three methods can be found in the Media Extensions associated with this paper. In the body-first method, the robot performed a 90° turn composed of three 30° turns. In the leg-first method, the robot performed four consecutive 20° turns. In the body/leg-simultaneous method, the 90° turn can be achieved by two 45° turns, as shown in the video, confirming that this method can be used for a large turning angle in each stride. In addition, different turn angles in each stride are used in the three different methods, confirming the capability of assigning an arbitrary turn angle when using the proposed methodology.

Fig. 11 shows the experimental snapshots of the robot performing simultaneous walking and turning. Snapshot in the middle of each sub-figure shows the top view of the robot motion recorded by another camcorder, revealing the COM motion on the horizontal plane. Complete videos of the above three methods can be found in the Media Extensions associated with this paper. At first, the robot is set to walk for two steps, then performs six 30° turns to complete a U-turn, and then walks for another two steps before standing still. These successful experimental results of robot motion confirm that the methodology of trajectory planning is functional and can be used in robot operation.

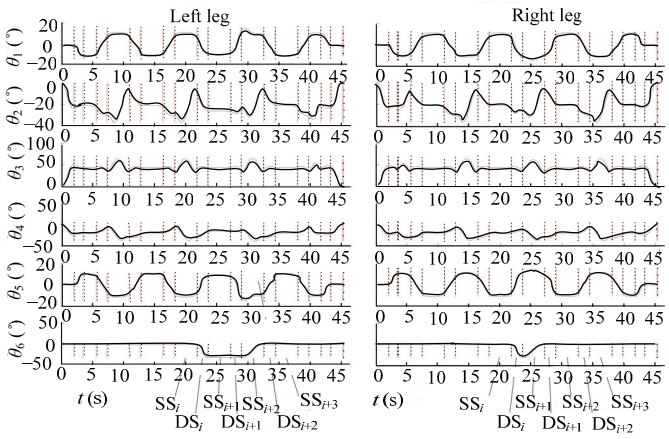

Fig. 9 Joint trajectories of the robot while it performs simultaneous walking and turning. Dotted lines indicate the timing of switches between SS phases and DS phases. The motion of simultaneous walking and turning is specifically marked.

Fig. 10 Sequential snapshots of the robot performing three different methods of turning in place. (a) Body-first; (b) leg-first; (c) body/leg-simultaneous. The robot configurations shown in snapshots 1–6 correspond to the motion steps from (b) to (g) discussed in section **2.1** and also shown in Fig. 3.

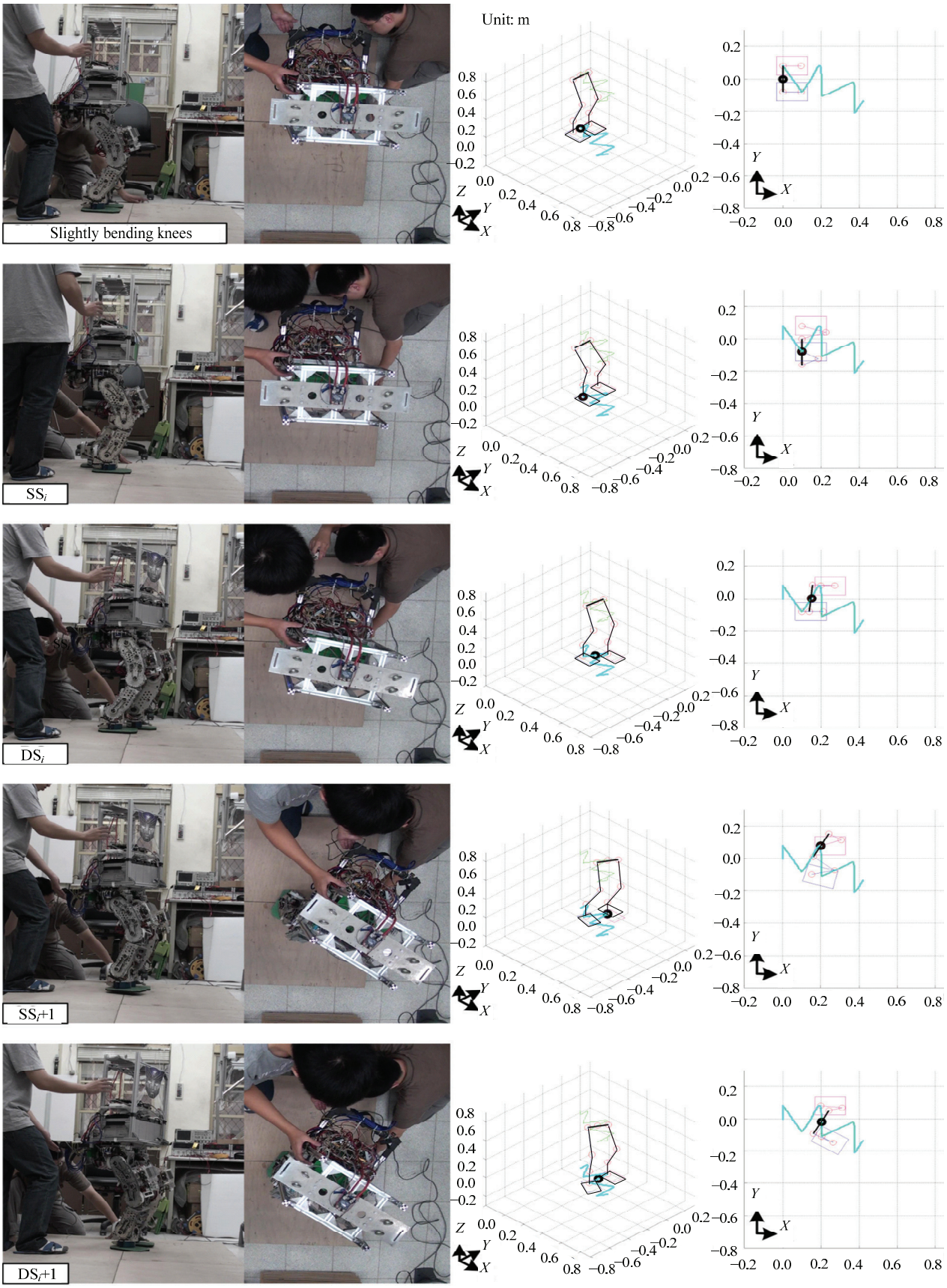

Fig. 11 Sequential snapshots of the robot performing simultaneous walking and turning. Robot configurations shown in the snapshots correspond to the key motion steps discussed in section **2.2** and also shown in Fig. 5.

4 Conclusion

We report on the development of turning in place behavior and simultaneous walking and turning behavior on a child-size bipedal robot. Three strategies for turning in place are investigated and compared. The body-first method is the best choice when walking follows turning immediately. The leg-first method is preferred when space behind the robot is very tight. The method of body/leg-simultaneous method is optimal when a large turning angle is desired. The design of the COM trajectory in simultaneous walking and turning is based on the linear inverted pendulum in the SS phase and on polynomial-based trajectory generation in the DS phase. Compared to straight walking, only two extra variables are introduced for simple computation: one is relative leg positioning angle, ϕ, and the other is scaling factor K. The former is used to determine the correct foot position for turning, and the latter adjusts the shape of the COM trajectory during critical body turning stages. Together with foot trajectories, joint trajectories can be derived by the inverse kinematic method. The methodology for planning turning trajectory was first designed in a simulation environment to make sure (1) that motion was stable by checking whether the ZMP trajectory thoroughly resided within the supporting region and (2) that joint trajectory was feasible to be executed in the empirical robot. After simulation, the trajectories were implemented on the child-size robot and experimental evaluation was conducted. Experimental results recorded on video confirm the effectiveness of the development of turning behavior.

Media Extensions

Eight movies are included in this paper, four made during simulation (the file names beginning with "Sim") and four made during experimentation (the file names beginning with "Exp"). In both simulation and experimentation, the robot operates in four turning methods, including three methods of turning in place and one method of simultaneous walking and turning. The movies are stored on a web page and can be accessed by clicking the following file names.

1	Sim_body-first.wmv
2	Sim_leg-first.wmv
3	Sim_body/leg-simultaneous.wmv
4	Sim_simultaneous-walking-and-turning.wmv
5	Exp_body-first.wmv
6	Exp_leg-first.wmv
7	Exp_body/leg-simultaneous.wmv
8	Exp_simultaneous-walking-and- turning.wmv

Acknowledgments

This work is supported by the National Science Council (NSC), Taiwan, under contract NSC 97-2221-E-002-208-MY3 and 100-2628-E-002 -021-MY3 as well as by the TSUNG Cho-Chang Education Foundation, Taiwan, under contract 101-S-A05.

References

[1] Imai T, Moore S T, Raphan T, Cohen B. Interaction of the body, head, and eyes during walking and turning. *Experimental Brain Research*, 2004, **136**, 1–18.

[2] Shih C L, Li Y Z, Churng S, Lee T T, Gruver W A. Trajectory synthesis and physical admissibility for a biped robot during the single-support phase. *IEEE International Conference on Robotics and Automation*. Cincinnati, USA, 1990, 1646–1652.

[3] Qiang H, Kajita S, Koyachi N, Kaneko K, Yokoi K, Arai H, Komoriya K, Tanie K. A high stability, smooth walking pattern for a biped robot. *IEEE International Conference on Robotics and Automation*, Detroit, USA, 1999, 65–71.

[4] Qiang H, Yokoi K, Kajita S, Kaneko K, Arai H, Koyachi N, Tanie K. Planning walking patterns for a biped robot. *IEEE Transactions on Robotics and Automation*, 2001, **17**, 280–289.

[5] Sugihara T, Nakamura Y. A fast online gait planning with boundary condition relaxation for humanoid robots. *IEEE International Conference on Robotics and Automation*, Barcelona, Spain, 2005, 305–310.

[6] Seung-Suk H, Jae-Hyoung Y, Young-Joon H, Hern-Soo H. Natural gait generation of biped robot based on analysis of human's gait. *International Conference on Smart Manufacturing Application*, Gyeonggi-do, Korea, 2008, 30–34.

[7] Chiang M H, Chang F R. Anthropomorphic design of the human-like walking robot. *Journal of Bionic Engineering*, 2013, **10**, 186–193.

[8] Luo X, Xu W L. Planning and control for passive dynamics

based walking of 3D biped robots. *Journal of Bionic Engineering*, 2012, **9**, 143–155.

[9] Hun-ok L, Takanishi A. Realization of continuous biped walking. *IEEE International Conference on Systems, Man, and Cybernetics*, Tucson, USA, 2001, 1630–1635.

[10] Kajita S, Kanehiro F, Kaneko K, Yokoi K, Hirukawa H. The 3D linear inverted pendulum mode: A simple modeling for a biped walking pattern generation. *IEEE/RSJ International Conference on Intelligent Robots and Systems*, Maui, USA, 2001, 239–246.

[11] Hu L Y, Zhou C J, Wu B, Yang T W, Yue Pik Kong. Locomotion planning and implementation of humanoid robot Robo-Eectus Senior (RESr-1). *IEEE-RAS International Conference on Humanoid Robots*, Pittsburgh, USA, 2007, 526–531.

[12] Yu Z G, Huang Q, Chen X C, Xu W, Li G, Li K J. On-line trajectory generation for a humanoid robot based on combination of off-line patterns. *ICIA International Conference on Information and Automation*, Zhuhai, China, 2009, 84–89.

[13] Kim E, Kim T, Kim J W. Three-dimensional modelling of a humanoid in three planes and a motion scheme of biped turning in standing. *IET Control Theory & Applications*, 2009, **3**, 1155–1166.

[14] Peng S J, Sui H T, Ma H X. A simulation and experiment research on turning gait planning of blackmann-II humanoid robot. *IEEE International Conference on Control and Automation* (*ICCA*), Xiamen, China, 2010, 719–724.

[15] Shi G Q, Wang H, Fang B F. Online omnidirectional walking patterns generation for biped robot. *International Conference on Electronic Measurement & Instruments*, Beijing, China, 2009, 856–861.

[16] Harada K, Miura K, Morisawa M, Kaneko K, Nakaoka S, Kanehiro F. Toward human-like walking pattern generator. *IEEE/RSJ International Conference on Intelligent Robots and Systems*, St. Louis, USA, 2009, 1071–1077.

[17] Miura K, Morisawa M, Nakaoka S, Kanehiro F, Harada K, Kaneko K, Kajita S. Robot motion remix based on motion capture data towards human-like locomotion of humanoid robots. *IEEE-RAS International Conference on Humanoid Robots*, Paris, France, 2009, 596–603.

[18] Nakaoka S, Nakazawa A, Yokoi K, Ikeuchi K. Leg motion primitives for a dancing humanoid robot. *IEEE International Conference on Robotics and Automation*, New Orleans, LA, USA, 2004, 610–615.

[19] Nakaoka S, Nakazawa A, Kanehiro F, Kaneko K, Morisawa M, Ikeuchi K. Task model of lower body motion for a biped humanoid robot to imitate human dances. *IEEE/RSJ International Conference on Intelligent Robots and Systems*, 2005, 3157–3162.

[20] Zhao X J, Huang Q, Peng Z Q, Li K J. Kinematics mapping and similarity evaluation of humanoid motion based on human motion capture. *Proceedings of IEEE/RSJ International Conference on Intelligent Robots and Systems*, Sendai, Japan, 2004, 840–745.

[21] ASIMO, Honda Motor Co, available at: http://asimo.honda.com/downloads/pdf/asimo-technical-information.pdf

[22] Sakagami Y, Watanabe R, Aoyama C, Matsunaga S, Higaki N, Fujimura K. The intelligent ASIMO: System overview and integration. *IEEE/RSJ International Conference on Intelligent Robots and System*s, 2002, **3**, 2478–2483.

[23] Miura K, Nakaoka S, Morisawa M, Kanehiro F, Harada K, Kajita S. Analysis on a friction based "twirl" for biped robots. *IEEE International Conference on Robotics and Automation* (*ICRA*), Alaska, USA, 2010, 4249–4255.

[24] K Miura, Kanehiro F, Kaneko K, Kajita S, Yokoi K. Quick slip-turn of HRP-4C on its toes. *IEEE International Conference on Robotics and Automation* (*ICRA*), Saint Paul, USA, 2012, 3527–3528.

[25] Hashimoto K, Yoshimura Y, Kondo H, Hun-ok L, Takanishi A. Realization of quick turn of biped humanoid robot by using slipping motion with both feet. *IEEE International Conference on Robotics and Automation* (*ICRA*), Shanghai, China, 2011, 2041–2046.

[26] Vukobratovic M, Borovac B. Zero-moment point- thirty five years of its life. *International Journal of Humanoid Robotics*, 2004, **1**, 147–173.

[27] Sugihara T, Nakamura Y, Inoue H. Real-time humanoid motion generation through ZMP manipulation based on inverted pendulum control. *Proceedings of IEEE International Conference on Robotics and Automation*, Washington, USA, 2002, 1404–1409.